Dalton Transactions

PAPER

View Article Online
View Journal | View Issue

Cite this: *Dalton Trans.*, 2015, **44**, 8255

Correlation between the molecular structure and the kinetics of decomposition of azamacrocyclic copper(II) complexes†

Laura Acosta-Rueda,‡[a] Estefanía Delgado-Pinar,‡[b] Javier Pitarch-Jarque,[b] Alexis Rodríguez,[b] Salvador Blasco,[b] Jorge González,[b] Manuel G. Basallote*[a] and Enrique García-España*[b]

The formation of copper(II) complexes with symmetrical dinucleating macrocyclic ligands containing two either monomethylated (**L1**) or trimethylated (**L2**) diethylenetriamine (Medien or Me3dien) subunits linked by pyridine spacers has been studied by potentiometry. Potentiometric studies show that **L1** has larger basicity than **L2** as well as higher stability of its mono- and binuclear complexes. The crystal structures of **L1**·6HCl (**1**), $[Cu_2(L1)Cl_2](CF_3SO_3)_2$ (**2**), $[Cu_2(L1)(OH)](ClO_4)_3{\cdot}3H_2O$ (**3**) and $[Cu(L1)](ClO_4)_2$ (**4**) show that **L1** adopts different coordination modes when bound to copper(II). Whereas in **2**, each copper(II) is bound to one Medien subunit and to one pyridine group, in **3** each metal center is coordinated to one 2,6-di(aminomethyl)pyridine moiety (damp) and to one aminomethyl group. The mononuclear complex **4** shows pseudo-octahedral coordination with two weakly coordinated axial nitrogens. Kinetic studies indicate that complex decomposition is strongly dependent on the coordination mode of **L1**. Upon addition of an acid excess, all the species except $[Cu_2(L1)]^{4+}$ convert very rapidly to an intermediate that decomposes more slowly to copper(II) and a protonated ligand. In contrast, $[Cu_2(L1)]^{4+}$ decomposes directly without the formation of any detectable intermediate. These results can be rationalized by considering that the crystal structures are maintained in solution and that the weakest Cu–N bonds are broken first, thus indicating that kinetic measurements on complex decomposition can be used to provide information about structural reorganizations in the complexes. In any case, complete decomposition of the **L1** complexes takes place in a maximum of two kinetically resolvable steps. However, minor changes in the structure of the complexes can lead to drastic changes in the kinetics of decomposition and the **L2** complexes decompose with polyphasic kinetics in which up to four different steps associated with the successive breaking of the different Cu–N bonds can be resolved.

Received 28th January 2015,
Accepted 26th March 2015

DOI: 10.1039/c5dt00408j

www.rsc.org/dalton

Introduction

The methylation of amino groups is a straightforward reaction that leads to derivatives exhibiting new chemical properties and reactivity. Due to the electron donor characteristics of the methyl group as well as due to alteration in the hydrogen bonding pattern, methylation promotes changes in the nucleophilicity and basicity of the amino groups. Moreover, methyl groups can provide important degrees of steric hindrance to the molecules. Substitution of N–H by N–CH_3 groups also inhibits oxidative dehydrogenation of the macrocycle,[1] which allows the preparation of complexes with an improved performance as models of non-heme oxygenases.[2] Partially methylated macrocycles have been also shown to be of interest. For instance, several years ago Lehn and coworkers showed that macrocycles as **L1** (see Scheme 1) are able to recognize pyruvate and catalyze H/D exchange at the methyl position.[3] Ligand **L1** can be considered as an example of a macrocyclic binucleating ligand with two symmetrical 3-nitrogen donor sets linked by spacers having one additional donor atom.[4] However, in this case there is some ambiguity about the defi-

[a]*Departamento de CMIM y Química Inorgánica, e Instituto de Biomoléculas (INBIO); Facultad de Ciencias, Universidad de Cádiz, Avda. República Saharahui s/n Puerto Real, 11510 Cádiz, Spain. E-mail: manuel.basallote@uca.es*

[b]*Instituto de Ciencia Molecular y Departamento de Química Inorgánica. Universidad de Valencia, C / Catedrático José Beltrán 2, 46980 Paterna, Valencia, Spain. E-mail: Enrique.garcia-Es@uv.es*

†Electronic supplementary information (ESI) available: Tables and figures with additional crystallographic, spectral and kinetic data. CCDC 1009322–1009325. For ESI and crystallographic data in CIF or other electronic format see DOI: 10.1039/c5dt00408j

‡These authors contributed equally.

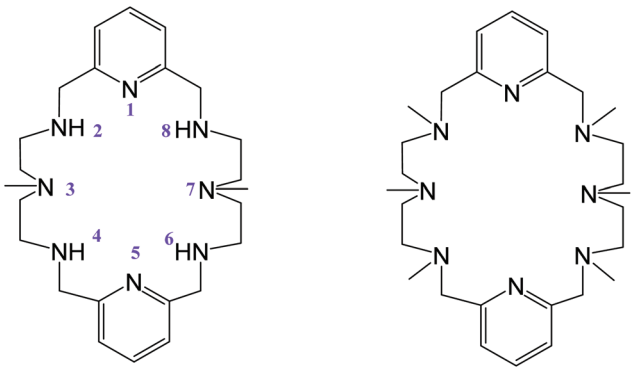

Scheme 1 Structures of **L1** (left) and **L2** (right) and the numbering of ligand **L1**.

nition of the donor sets and the spacers, so that the ligand can be considered to consist either of two partially methylated diethylenetriamine (Medien) subunits linked by pyridine-containing spacers or of two 2,6-di(aminomethyl)pyridine (damp) subunits linked by spacers containing tertiary N–CH_3 amino groups. In the present work, we compare the properties of **L1**, and its copper(II) complexes, with those of the related ligand **L2**, which contains trimethylated diethylenetriamine subunits (Me3dien) instead of Medien. In general, this kind of ligand is known to form stable mono and binuclear species and there is an abundant body of literature about the stability of the species formed. Although there is also abundant information about the structure of the complexes formed, there are not many cases in which the crystal structures of both mono and binuclear species are both known for the same system. In the present case, the structures of up to three different complexes of **L1** with the same metal ion (Cu^{2+}) have been solved, which provides an excellent opportunity to analyze the way in which different coordination modes of the ligand affect the kinetics of complex decomposition. Indeed, understanding the kinetics of the acid-promoted decomposition of copper complexes is fundamental when thinking of possible biological applications of these compounds, either in therapy[5] or diagnosis with radioactive ^{64}Cu.[6] Decomposition of a metal complex with a coordinated polyamine involves necessarily several steps, at least one for dissociation and protonation of each coordinated nitrogen atom. However, it has for long been known that these processes usually occur with monophasic kinetics in which the rate-limiting step corresponds to dissociation of the first metal–nitrogen bond, although in some cases it is displaced to the breaking of the second Cu–N bond.[7] A few cases of polyphasic kinetics are also found in the literature, especially when one of the bonds is very labile.[8] More importantly, the rates of complex decomposition span over a very wide range, from cases in the faster limit of the stopped-flow to cases in which the process requires days in the presence of a large excess of acid. On the basis of kinetic data for different complexes, the lability of a given complex has been associated with the strain of the Cu–N bonds,[9] but there is no precise literature information for the sequence of bond breaking within a given complex. The data in the present paper for the Cu–**L1** complexes provide such information and indicate that the sequence can be deduced from the crystal structures of the species, confirming that the weakest axial bonds are broken first. Moreover, species with different coordination modes can show different kinetics of decomposition, and this can be used to reveal structural changes for a given metal–ligand system. Although we have reported a few cases of such kinetic differences within a series of closely related species,[10] it is only in the present case that the availability of several crystal structures has allowed a clear correlation between the structure and the sequence of bond breaking. The decomposition of the Cu–**L2** complexes also shows a striking kinetic behavior in which the Cu–N bonds are sequentially broken in different kinetically-resolvable steps, which leads to polyphasic kinetics with an extremely unusual number of resolved steps.

Results and discussion

Speciation studies: protonation constants

As is perceptive for polyamine ligands, protonation constants need to be calculated before performing any other speciation study (Table 1). Potentiometric data indicate that **L1** and **L2** present five measurable protonation constants. The electrostatic repulsion introduced into the macrocycle by the presence of five ammonium groups prevents calculating the sixth protonation constant in the 2.5–11.0 pH range available for potentiometric studies. While the first four constants are relatively high with values arranged in groups of two, the fifth one is much reduced. In the case of **L1**, taking into account similar systems and the basicity of amino groups in water,[11] the first four protonation steps should involve the secondary amino groups of the polyamine, and the fifth one a methylated amine.

The hexamethylated ligand **L2** displays lower overall cumulative basicity ($\log\beta$, Table 1) and lower basicity in all the protonation steps, except the first one. This reduction in basicity can be attributed to the poorer solvating capacity of the tertiary

Table 1 Logarithms of the stepwise protonation constants of **L1** and **L2** determined in 0.15 M NaCl at 298.1 ± 0.1 K

	$\log K$	
Reaction	**L1**	**L2**
$L + H^+ \rightleftarrows HL^+$	9.09(2)[a]	9.45(2)
$HL^+ + H^+ \rightleftarrows H_2L^{2+}$	8.58(2)	8.27(2)
$H_2L^{2+} + H^+ \rightleftarrows H_3L^{3+}$	7.70(3)	6.97(3)
$H_3L^{3+} + H^+ \rightleftarrows H_4L^{4+}$	7.45(3)	5.77(3)
$H_4L^{4+} + H^+ \rightleftarrows H_5L^{5+}$	3.28(5)	3.12(3)
$\log\beta$[b]	36.1	33.6

[a] Numbers in parentheses are standard deviations in the last significant figure. [b] Cumulative basicity constant $\beta = \sum K_{H_jL}$.

amino groups in water that does not compensate for the electron donor characteristic of the methyl groups.[11a]

Copper(II) stability constants

The stability constants for the formation of copper(II) complexes of **L1** and **L2** determined in 0.15 M NaCl at 298.1 K are shown in Table 2. Speciation studies show the formation of mononuclear and binuclear complexes of $[Cu(H_xL)]^{(2+x)+}$ (x = 0–2 for **L1** and x = 0–3 for **L2**) and $[Cu_2(H_xL)]^{(4+x)+}$ (x = 0–2 for **L1** and **L2**) stoichiometries, respectively. A mononuclear hydroxylated species $[Cu(L1)(OH)]^{+}$ was also detected for **L1** and binuclear hydroxylated species $[Cu_2(L)(OH)_x]^{(4-x)+}$ (x = 1,2) are also formed for both ligands at basic pHs. The distribution diagrams for the system Cu : **L1** (Fig. 1A and 1B) show that while for a 1 : 1 Cu : **L1** molar ratio the binuclear species prevail below pH = 5 and the mononuclear ones above this pH, for a 2 : 1 Cu : **L1** molar ratio the binuclear species prevail throughout the pH window explored. In the case of **L2** a clearcut separation is observed, with the mononuclear species essentially predominating for a 1 : 1 Cu : **L2** molar ratio and the binuclear ones for a 2 : 1 Cu : **L2** molar ratio.

Regarding the mononuclear complexes of **L1**, the number of protonated species is the same as the number of unbound nitrogen atoms in the crystal structure of $[Cu(L1)](ClO_4)_2$ (**1**) (see below). The values obtained for the stepwise protonation constants of the mononuclear complexes suggest that such protonations are occurring at the unbound secondary and tertiary amino groups of the crystal structure. On the other hand, the value of the formation constant of $[Cu(L1)]^{2+}$ lies between those previously reported for the unmethylated pyridinophane **L3** ($\log K$ = 20.9) and for the related ligand **L4** containing propylenic instead of ethylenic chains in the bridges ($\log K$ = 16.30) (see Scheme 2).[7] Finally, the low tendency of the $[Cu(L1)]^{2+}$ species to hydrolyze ($\log K$ = −11.34) suggests that the process requires the cleavage of a Cu–N bond.[3,12]

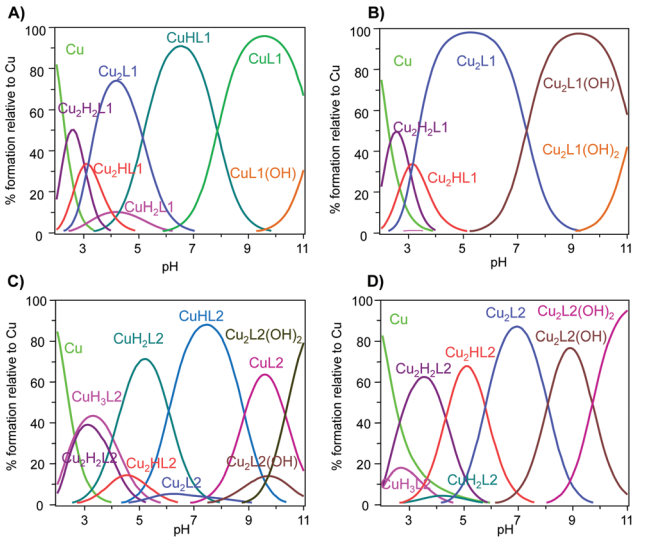

Fig. 1 Distribution diagram of (A) $[Cu^{2+}]$ = [**L1**] = 0.001 M, (B) $[Cu^{2+}]$ = 0.002 M, [**L1**] = 0.001 M, (C) $[Cu^{2+}]$ = [**L2**] = 0.001 M, and (D) $[Cu^{2+}]$ = 0.002 M, [**L2**] = 0.001 M.

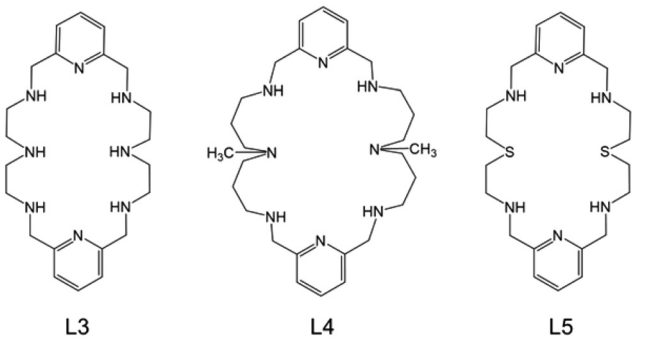

Scheme 2 Ligands **L3**, **L4** and **L5**.

Table 2 Logarithms of the stability constants for the systems Cu^{2+}–**L1** and Cu^{2+}–**L2** determined at 298.1 ± 0.1 K in 0.15 M NaCl

	$\log K$	
Reaction	**L1**	**L2**
$[Cu(H_2L)]^{4+} + H^+ \rightleftarrows [Cu(H_3L)]^{5+}$		4.03(4)
$[Cu(HL)]^{3+} + H^+ \rightleftarrows [Cu(H_2L)]^{4+}$	4.29(2)[a]	6.08(4)
$[Cu(L)]^{2+} + H^+ \rightleftarrows [Cu(HL)]^{3+}$	7.78(3)	8.84(5)
$Cu^{2+} + L \rightleftarrows [Cu(L)]^{2+}$	18.23(2)	12.80(4)
$Cu^{2+} + L + H_2O \rightleftarrows [Cu(L)(OH)]^{+} + H^+$	−11.34(2)	
$2Cu^{2+} + L \rightleftarrows [Cu_2(L)]^{4+}$	29.07(4)	22.15(4)
$[Cu_2(HL)]^{5+} + H^+ \rightleftarrows [Cu_2(H_2L)]^{6+}$	3.02(1)	4.33(3)
$[Cu_2(L)]^{4+} + H^+ \rightleftarrows [Cu_2(HL)]^{5+}$	3.16(2)	5.78(4)
$[Cu(L)]^{2+} + Cu^{2+} \rightleftarrows [Cu_2(L)]^{4+}$	10.84(2)	9.35(4)
$[Cu_2(L)]^{4+} + H_2O \rightleftarrows [Cu_2(L)(OH)]^{3+} + H^+$	−7.32 (2)	−8.07(4)
$[Cu_2(L)(OH)]^{3+} + H_2O \rightleftarrows [Cu_2(L)(OH)_2]^{2+} + H^+$	−11.14 (1)	−9.73(7)

[a] Numbers in parentheses are standard deviations in the last significant figure.

The constant for the formation of the mononuclear complex of **L2** $[CuL2]^{2+}$ ($\log K$ = 12.80(3)) is much lower than that of the corresponding complex of **L1** and also than those of **L3** and **L4** just commented on. Even if the basicity of **L2** is smaller than that of **L1**, its lower stability constants yield lower pCu^{2+} values ($pCu^{2+} = -\log[Cu^{2+}]_{free}$) over the whole pH range where complexation occurs (Fig. S5†). This reduction in stability may be due, apart from to the poorer donating ability of the tertiary amines,[13] to a lower coordination number. The bulky methyl groups would impede the approach of enough nitrogen donors to complete the hexa-coordination. As a matter of fact, in this system while a further protonated species ($[Cu(H_3L2)]^{5+}$) can be found, the stepwise protonation constants of the mononuclear species are significantly higher

than those of the corresponding mononuclear complexes of **L1**.

With respect to the stability constants of the binuclear complexes, the first point that deserves comment is the low values of the protonation constants of the binuclear species, suggesting that the protonation is accompanied by the breaking of a Cu–N bond. The close values between both protonation steps may indicate that each one takes place in a different copper center. The value for the formation of the $[Cu_2(L1)]^{4+}$ species ($\log K$ = 29.07) is again smaller than that found for **L3** ($\log K$ = 33.48) and slightly higher than the one reported for **L4** ($\log K$ = 28.48),[14] but much higher than the one for the fully methylated ligand, $[Cu_2(L2)]^{4+}$ ($\log K$ = 22.15(4)). As happens for the mononuclear complexes, the protonation constants of the binuclear complexes of **L2** are markedly higher than those of **L1**. On the other hand, the hydrolytic constant of the $[Cu_2(L)]^{4+}$ species ($\log K$ = −7.32 for $[Cu_2(L1)]^{4+}$) ($\log K$ = −8.07 for $[Cu_2(L2)]^{4+}$) agrees with the bridging mode of the hydroxo ligand evidenced in the crystal structure of compound **3** commented below.

Crystal structure of $[H_6L1]Cl_6{\cdot}6H_2O$ (1)

The crystal structure of **1** is formed by H_6L1^{6+} cations (see Fig. 2), chloride anions which counter-balance the positive charges, and water molecules. Crystallographic details of the crystal structures are shown in Table S1.† The macrocycle presents the four secondary amino groups and the two methylated nitrogens protonated. As usually happens in related pyridinophane macrocycles, the pyridine nitrogen atoms remain unprotonated. The hexavalent cation, which has an inversion center, displays a sort of staircase shape with the step being formed by the tertiary amines. Table S2† includes the torsion angles along the bridge. The distance between the centroid of one of the pyridine rings and the plane that goes through the other one is 1.90 Å. The chloride anions participate in a hydrogen bonding network that involves the protonated ammonium groups and water molecule (Table S3 and Fig. S1†).

Crystal structure of $[Cu_2(L1)Cl_2](CF_3SO_3)_2$ (2)

The crystal structure of **2** consists of $[Cu_2(L1)Cl_2]^{2+}$ binuclear cations and $CF_3SO_3^-$ counter-anions. The copper sites within the binuclear complexes are related by an inversion center. Each copper(II) presents a square pyramidal geometry in which the equatorial plane is defined by two secondary amines, a tertiary amine and a chloride anion. Interestingly, and differently from what it is more frequently found in copper(II) complexes of pyridine containing macrocycles,[3,15,16] the pyridine nitrogen donors are placed at the axially elongated apical positions of the square pyramid (Table 3, Fig. 3).

Also of interest is that, for this to occur, the nitrogen atoms contiguous to a pyridine ring are not both involved in the binding of the same metal ion, being the sequence of coordinated nitrogen atoms N_s, N_t, N_s, N_{pyr} (s = secondary, t = tertiary, pyr = pyridine). In the binuclear units the distance between the metals is 5.5957(8) Å. The binuclear cation displays a sort of twisted-chair conformation with the pyridine rings and the copper atoms located in the same plane. The different binuclear units are interconnected by four hydrogen bonds involving the coordinated chloride anions as acceptors and amino groups N2–H as donors (Fig. S2 and Table S4†).

Table 3 Selected bond distances (Å) and angles (°) for **2**

Bond distances (Å)		Bond angles (°)	
Cu1–N1	2.061(3)	Cl1–Cu1–N1	98.15(6)
Cu1–N2	2.101(3)	N3–Cu1–Cl1	163.55(7)
Cu1–N3	1.951(3)	N3–Cu1–N1	97.24(8)
Cu1–N4	2.012(4)	N4–Cu1–Cl1	91.74(6)
Cu1–Cl1	2.332(4)	N4–Cu1–N3	85.36(8)
		N4–Cu1–N1	120.73(8)
		N2–Cu1–Cl1	92.30(6)
		N2–Cu1–N3	85.25(8)
		N2–Cu1–N4	160.06(9)
		N2–Cu1–N1	77.93(8)

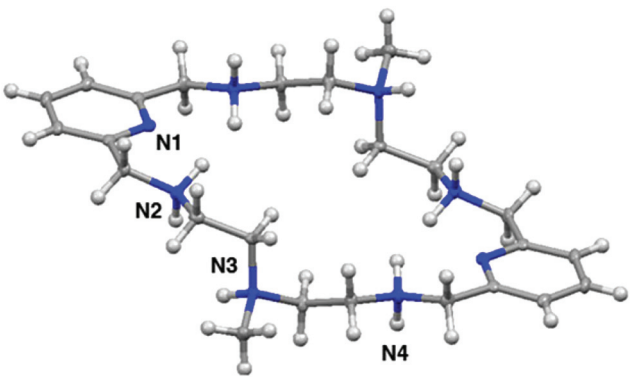

Fig. 2 Ellipsoid drawing of the $[H_6L1]^{6+}$ cation (the thermal ellipsoids are set at 50% probability).

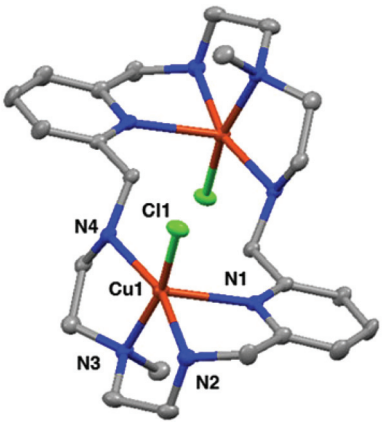

Fig. 3 Ellipsoid representation of the $[Cu_2(L1)Cl_2]^{2+}$ complex cation (the thermal ellipsoids are set at 50% probability). Hydrogen atoms are not shown.

Crystal structure of $[Cu_2(L1)(OH)](ClO_4)_3{\cdot}3H_2O$ (3)

The asymmetric unit of **3** consists of $[Cu_2(L1)(OH)]^{3+}$ cations, perchlorate counter-anions and lattice water molecules. Each binuclear cation includes two slightly different copper sites with distorted square pyramidal geometry, the values of the Addison τ parameter are 0.39 and 0.38 for Cu(1) and Cu(2),[17] respectively. In contrast to **2**, the pyridine rings are in this case occupying equatorial positions, which are completed by the two secondary amines contiguous to the pyridine and the hydroxo bridging ligand. The axial positions in both metal sites are occupied by the tertiary amino groups. The shortest distances in the equatorial planes lie in the axis connecting the two pyridine rings through the hydroxo bridge (Table 4, Fig. 4). The distance between the copper(II) ions is 3.6421(7) Å and the Cu–O–Cu angle is 145.6°. Also, in contrast to the previous structure, the more frequent $N_sN_{py}N_s$ sequence (damp) of nitrogen donors in the equatorial plane occurs here. The planes passing through the pyridine rings form an angle of 46°. A somewhat similar structure was reported for **L5** having thioether groups instead of methylated nitrogens at the central positions of the chains in which the sulfur atoms were weakly coordinating the metal ions.[18]

Table 4 Selected bond distances (Å) and angles (°) for **3**

Bond distances (Å)		Bond angles (°)	
Cu1–O1	1.908(3)	O1–Cu1–N2	100.87(14)
Cu1–N2	2.063(4)	O1–Cu1–N1	178.63(14)
Cu1–N1	1.937(4)	O1–Cu1–N8	97.91(14)
Cu1–N8	2.068(4)	O1–Cu1–N7	94.53(12)
Cu1–N7	2.459(4)	N2–Cu1–N8	155.60(16)
Cu2–O1	1.903(3)	N2–Cu1–N7	111.95(16)
Cu2–N5	1.939(3)	N1–Cu1–N2	78.44(16)
Cu2–N4	2.058(4)	N1–Cu1–N8	82.44(16)
Cu2–N6	2.075(4)	N1–Cu1–N7	86.83(13)
Cu2–N3	2.529(4)	N8–Cu1–N7	81.73(14)
		O1–Cu2–N5	178.59(15)
		O1–Cu2–N4	98.81(14)
		O1–Cu2–N6	100.15(13)
		N5–Cu2–N4	82.24(15)
		N5–Cu2–N6	79.10(14)
		N4–Cu2–N6	155.59(15)
		N3–Cu2–O1	92.34(14)
		N6–Cu2–N3	115.09(15)
		N5–Cu2–N3	86.95(14)
		N4–Cu2–N3	79.23(16)

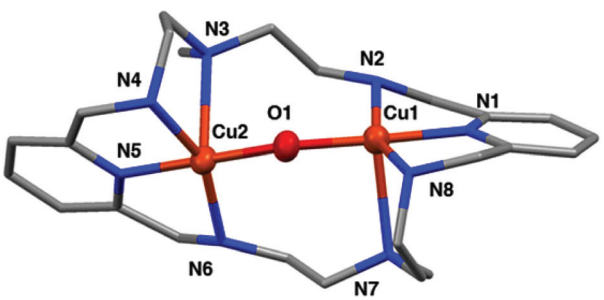

Fig. 4 Stick representation of the $[Cu_2(L1)(OH)]^{3+}$ complex cation. Hydrogen atoms are not shown.

Crystal structure of the mononuclear $[Cu(L1)](ClO_4)_2$ (4)

The crystal structure of **4** is formed by $[Cu(L1)]^{2+}$ cations, perchlorate counter-anions and lattice water molecules. Interestingly, the synthesis of the 1 : 1 complex could be easily achieved because, as shown in the distribution diagrams, when mixing aqueous solutions of copper(II) and **L1** in a 1 : 1 molar ratio the mononuclear species prevail in solution above pH 6 without any interference from the binuclear complexes. The coordination geometry can be defined either as square pyramidal with the nitrogen atom of the second pyridine unit pointing towards the metal ion or as a strongly distorted octahedron. The equatorial plane is defined by the nitrogen of one of the pyridines, the two contiguous secondary amino groups and by one of the amino groups contiguous to the other pyridine subunit (Fig. 5, Table 5). A tertiary amino group (N3) and the pyridine nitrogen N5 are placed at the strongly elongated axial positions of the octahedron. In this structure, the second methylated nitrogen and one secondary amino group remain uncoordinated.

The macrocycle adopts a twisted conformation with the metal ion completely occluded in its interior (Fig. 5, right). The angle between the planes of the pyridine rings is almost normal (87°).

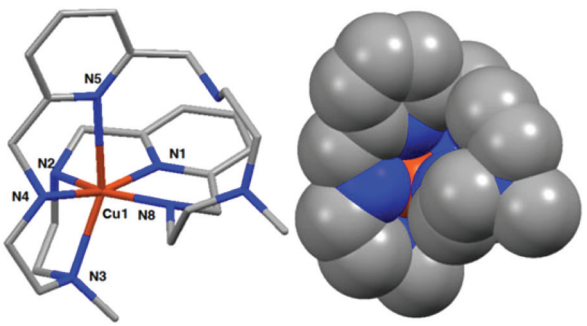

Fig. 5 Stick representation (left) and space-fill view (right) of the $[Cu(L1)]^{2+}$ complex cation. Hydrogen atoms are not shown.

Table 5 Selected bond distances (Å) and angles (°) for crystals **4**

Bond distances (Å)		Bond angles (°)	
Cu1–N8	2.061(3)	N8–Cu1–N2	159.31(14)
Cu1–N2	2.101(3)	N8–Cu1–N3	103.87(12)
Cu1–N1	1.951(3)	N2–Cu1–N3	80.91(14)
Cu1–N4	2.012(4)	N1–Cu1–N8	80.28(12)
Cu1–N3	2.332(4)	N1–Cu1–N2	79.43(14)
Cu1–N5	2.740 (4)	N1–Cu1–N4	163.72(16)
		N1–Cu1–N3	113.88(15)
		N4–Cu1–N8	100.61(13)
		N4–Cu1–N2	99.99(15)
		N4–Cu1–N3	81.86(17)

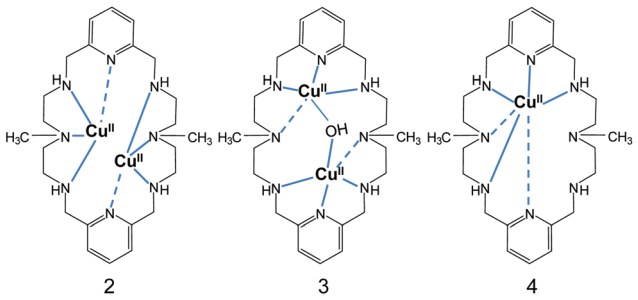

Fig. 6 Schematic representation of the coordination mode adopted by **L1** in complexes **2**, **3** and **4**. Dotted lines stand for the axial bonds.

As a summary, the different coordination sequences depicted in Fig. 6 have been observed.

While in **2** the nitrogen donor of the pyridine ring is placed at the axial position, in the other two structures the methylated nitrogen occupies such a position. In other words, in **2** we have a methylated diethylenetriamine (Medien) moiety and a chloride in the equatorial position, while in the other two structures a di(aminomethyl)pyridine (damp) plus a hydroxyl or a secondary amino group fill the equatorial plane. As discussed below these differences are key points to explain the kinetics and molecular reorganizations observed along the dissociation mechanisms of the complexes.

The kinetics of acid-promoted complex decomposition of Cu–L1 complexes

According to the species distribution curves, addition of an excess of acid to a solution containing the metal complexes results in complex decomposition with formation of Cu^{2+} and H_5L^{5+} (eqn (1)). The kinetics of this process can be measured by monitoring the disappearance of the absorption band of the complex. However, to avoid complications caused by the existence of mixtures of species in solution, it is convenient to carry out the measurements starting with solutions containing a single complex species.[19] By using this strategy, it has been previously found that these studies not only provide information about the acid-promoted decomposition of the complex but also they can even reveal the existence of structural reorganizations. In the case of **L1**, the species distribution curves (Fig. 1) indicate that an adequate selection of the experimental conditions for the starting solutions (different pH values and Cu : **L1** ratios of 1 : 1 and 2 : 1) allows studying the kinetics of decomposition starting from solutions containing the $[Cu(HL1)]^{3+}$, $[Cu(L1)]^{2+}$, $[Cu_2(L1)]^{4+}$ and $[Cu_2(L1)(OH)]^{3+}$ species, which reach more than 90% of the total species content under specific conditions of pH and Cu : **L1** molar ratio. Although the binuclear $[Cu_2(H_2L1)]^{6+}$ complex does not reach such high percentages, its kinetics of decomposition could also be studied because solutions with a 2 : 1 Cu : **L1** molar ratio contain at low pH values only this species in equilibrium with Cu^{2+}, which does not interfere with the decomposition process. In contrast, the decomposition of the $[Cu(L1)(OH)]^{+}$ and $[Cu_2(L1)(OH)_2]^{2+}$ hydroxo species formed at very high pH could not be studied due to their scarce solubility under the experimental conditions used.

$$[Cu_y(H_xL)(OH)_z]^{(x+2y-z)+} + H^+_{exc} \rightarrow yCu^{2+} + H_5L^{5+} \quad (1)$$

Monitoring the kinetics of decomposition at multiple wavelengths using a stopped-flow instrument equipped with a diode-array detector allows a comparison of the spectrum recorded immediately upon mixing with that recorded in the absence of acid. The lack of coincidence between both spectra indicates the existence of rapid processes occurring within the stopped-flow mixing time (*ca.* 1.7 ms for the instrument used). In the decomposition of the mononuclear $[Cu(HL1)]^{3+}$ and $[Cu(L1)]^{2+}$ species, as well as for the binuclear $[Cu_2(L1)(OH)]^{3+}$, the absorption band is shifted within the mixing time from the wavelengths indicated in Table 6 to 700 nm (Fig. 7), thus showing the existence of a rapid step whose rate constants (k_{1obs}) cannot be measured. Stopped-flow experiments at

Table 6 Position and intensity of the absorption band and kinetic data for the second kinetic step observed in the acid-promoted decomposition of the different mono and binuclear Cu^{2+}-**L1** species

Complex	λ_{max}/nm	ε/M^{-1} cm^{-1}	a/s^{-1}	b/M^{-1} s^{-1}
$[Cu(HL1)]^{3+}$	650[a]	172	0.4 ± 0.1	29 ± 4
$[Cu(L1)]^{2+}$	645[a]	118	—	30 ± 1
$[Cu_2(H_2L1)]^{6+}$	700	238	1.0 ± 0.1	25 ± 1
$[Cu_2(L1)(OH)]^{3+}$	645[a]	156	1.1 ± 0.1	32 ± 2
$[Cu_2(L1)]^{4+}$	650[b]	398	0.14 ± 0.02	5.2 ± 0.3

[a] The band is shifted to 700 nm within the mixing time of the stopped-flow instrument. [b] For this complex this is the only kinetic step observed.

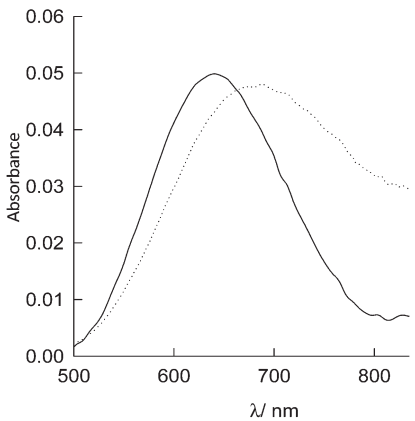

Fig. 7 Electronic spectra for a 2 × 10^{-4} M solution of $[Cu(HL1)]^{3+}$ in 0.15 M NaCl at pH = 6.20 (continuous), and the spectrum obtained immediately upon mixing that HCl solution to achieve a total concentration of acid of 0.08 M (dots). The spectra have been scaled to consider the dilution achieved in the stopped-flow instrument.

298.1 ± 0.1 K also show slower spectral changes (Fig. 8) that lead to complete decomposition of the intermediate formed in the rapid step. Those changes can be fitted by a kinetic model with a single step that leads to rate constants (k_{2obs}) whose dependence with the acid concentration (Fig. 9 and S4†) is given by eqn (2) with the values of the a and b parameters given in Table 6. As indicated in Fig. 9 and Table 6, the diprotonated $[Cu_2(H_2L1)]^{6+}$ species decomposes with kinetics similar to $[Cu_2(L1)(OH)]^{3+}$.

$$k_{obs} = a + b[H^+] \quad (2)$$

However in this case no shift in the absorption band is observed within the stopped-flow mixing time because the starting complex already shows the absorption band at 700 nm. The rate law in eqn (2) has been frequently observed in the literature and interpreted in terms of parallel attacks by water and proton to an activated intermediate resulting from the partial dissociation of one Cu–N bond.[20] Fig. 9 and S4† show that the kinetic data are very similar in experiments starting with any of the $[Cu(HL1)]^{3+}$, $[Cu(L1)]^{2+}$, $[Cu_2(H_2L1)]^{6+}$ and $[Cu_2(L1)(OH)]^{3+}$ species, thus showing that the equilibria involving these species are rapidly established and all of them decompose through a common reaction pathway. Actually, the four sets of data could be ascribed to the decomposition of the same intermediate, the differences being attributable to accumulation of experimental and fitting errors.

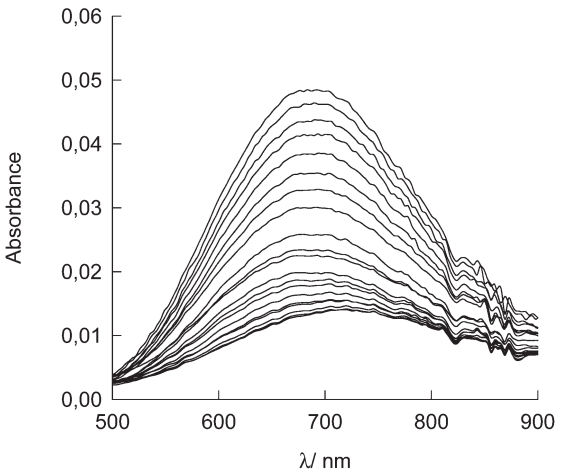

Fig. 8 Spectral changes with time for the disappearance of the band at 700 nm generated within the stopped-flow mixing time in the decomposition of the $[Cu(HL1)]^{3+}$ species.

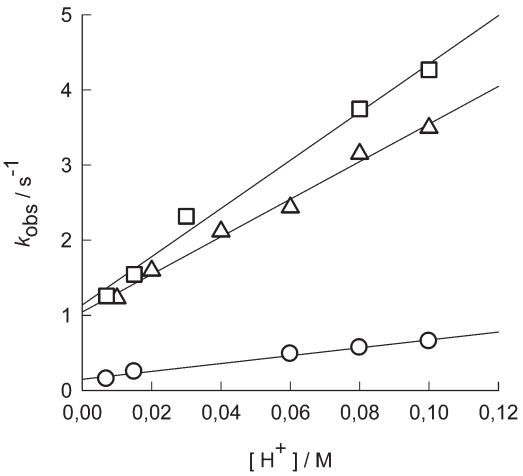

Fig. 9 Plot of the acid dependence for the observed rate constant corresponding to the second step in the acid-promoted decomposition of the $[Cu_2H_2(L1)]^{6+}$ (triangles) and $[Cu_2(L1)(OH)]^{3+}$ (squares) species, and for the single kinetic step observed in the decomposition of $[Cu_2(L1)]^{4+}$ (circles).

This common intermediate, with an absorption band centred at 700 nm and a molar absorptivity of *ca.* 300 M^{-1} cm^{-1}, must be a mononuclear species with a higher protonation state, *i.e.* $[Cu(H_xL1)]^{(2+x)+}$ with $x \geq 2$. Unfortunately, $[Cu(H_2L1)]^{4+}$ is always a minor species and its spectrum cannot be satisfactorily measured, so that a precise determination of the protonation state of the intermediate is not possible. However, if it is assumed that the structure of the $[Cu(L1)]^{2+}$ species in solution is equivalent to that solved by X-ray diffraction, addition of two protons to the uncoordinated amine groups is expected to be fast but it should not lead to large changes in the spectrum because the coordination environment around copper would be maintained. As the experimental data show a significant shift of the absorption band, it can be concluded that the rapid kinetic step involves the breaking of at least one Cu–N bond, so that the intermediate contains at least three protons.

Fig. 9 shows that the only species with a significantly different decomposition kinetics is $[Cu_2(L1)]^{4+}$. Although the complex shows a band at 650 nm, no spectral changes are observed within the mixing time for its reaction with acid, decomposition occurring in a single kinetic step with rate constants smaller than those observed for the intermediate formed from the other species. Moreover, although the data can be also fitted by eqn (2), the values of *a* and *b* are significantly different from those observed for the other species.

The similarity in the kinetics of decomposition of all the species except $[Cu_2(L1)]^{4+}$ indicates that those species decompose through intermediates with the same coordination environment of the metal centre. If it is assumed again that the crystal structures are maintained in solution, formation of the intermediate from $[Cu_2(L1)(OH)]^{3+}$ should involve the breaking of the OH^- bridge and surely at least one of the Cu–N bonds, given the shift of the absorption band. The crystal structure of the binuclear hydroxo complex indicates that the axial Cu–N3 bond is about 0.5 Å longer than the other Cu–N bonds, so it can be assumed that this is the first bond to be broken upon rapid protonation. This leads to the conclusion that the intermediates with the band centred at 700 nm most likely contain copper coordinated to a 2,6-di(aminomethyl)-pyridine (damp) fragment. In the case of the mononuclear $[Cu(L1)]^{2+}$ complex, decomposition is expected to occur with

initial attack to the weaker Cu–N bond, in this case that with the very loosely coordinated pyridine N5, and surely also with N3. However, dissociation of both groups would facilitate dissociation of the Cu–N4 bond because it would be no longer implied in the formation of chelate rings. As a result, rapid formation of an intermediate containing copper(II) coordinated to a damp fragment could be also justified in this case. According to this model, $[Cu_2(H_2L1)]^{6+}$ should contain two copper(II) ions coordinated to damp fragments and the two protons would be located at the aminomethyl groups. Consequent to this structure, the absorption band for the complex appears at 700 nm.

Interestingly, the only species which is unable to undergo direct conversion to an intermediate containing this fragment is $[Cu_2(L1)]^{4+}$, and this is the only species showing different kinetics of decomposition. According to its crystal structure, formation of an intermediate containing copper coordinated to a damp fragment would require the formation of a bond with N8, but the formation of Cu–N bonds is very unlikely in the presence of a large excess of acid.

Moreover, the crystal structure shows that the longer Cu–N bond is now with the pyridine group, so that if decomposition starts with acid attack at this site it would result in the formation of an intermediate with copper(II) coordinated to a Medien fragment. As $[Cu(dien)]^{2+}$ and copper(II) complexes with binucleating ligands containing dien fragments are known to decompose with kinetics faster than that observed for $[Cu_2(L1)]^{4+}$,[21,22] the intermediate generated upon the initial protonation of the pyridine nitrogen would be undetectable, in agreement with the experimental observations. Fig. 10 summarizes the model described above. All the species whose structure contains Cu^{2+}–damp fragments would decompose through detectable intermediates containing that group. In contrast, $[Cu_2(L1)]^{4+}$ cannot form those fragments in the presence of acid excess and it decomposes through an undetectable intermediate with Cu^{2+}–Medien fragments. The validity of this model was confirmed by additional experiments aimed at monitoring the interconversion between the different species. According to Fig. 10, protonation of the mononuclear $[Cu(L1)]^{2+}$ species and deprotonation of $[Cu(HL1)]^{3+}$ should be fast processes because they involve exclusively an uncoordinated amino group. These expectations were confirmed by stopped-flow experiments in which solutions containing one of both species were mixed with a buffer (MOPS or borate) with the pH required to force conversion to the other species. Those experiments showed that all the spectral changes occur within the mixing time and consist in changes in the position and intensity of the absorption band that agree well with the values in Table 6. Similar experiments using $[Cu_2(L1)]^{4+}$ showed that its conversion to $[Cu_2(L1)(OH)]^{3+}$ is slower (Fig. S4†), and a rate constant of 59 ± 5 s^{-1} could be measured at pH 9.50. The reverse process also occurs in the stopped-flow time scale (Fig. S5†), formation of $[Cu_2(L1)]^{4+}$ occurring with a rate constant of 0.39 ± 0.01 s^{-1} at pH = 5.30 (MES buffer). The observation of measurable kinetic steps for the interconversion of these species is in agreement with the changes required in the coordination environment of the metal centres. Similar studies involving $[Cu_2(L1)]^{4+}$ and $[Cu_2(H_2L1)]^{6+}$ were not so clear, probably because of some interaction with the buffer and of the formation of significant amounts of $[Cu_2(HL1)]^{5+}$. In any case, the spectral changes observed for the reaction of $[Cu_2(L1)]^{4+}$ with a buffer at pH = 2.7 (formic/formate) yielded a rate constant of 0.16 ± 0.03 s^{-1}, whereas a value of 4 ± 1 s^{-1} could be derived for the reverse process. Although some interference from the reaction with the buffering agent cannot be ruled out, the observation of measurable kinetic steps is again in agreement with the changes in the coordination environment required for the model in Fig. 10.

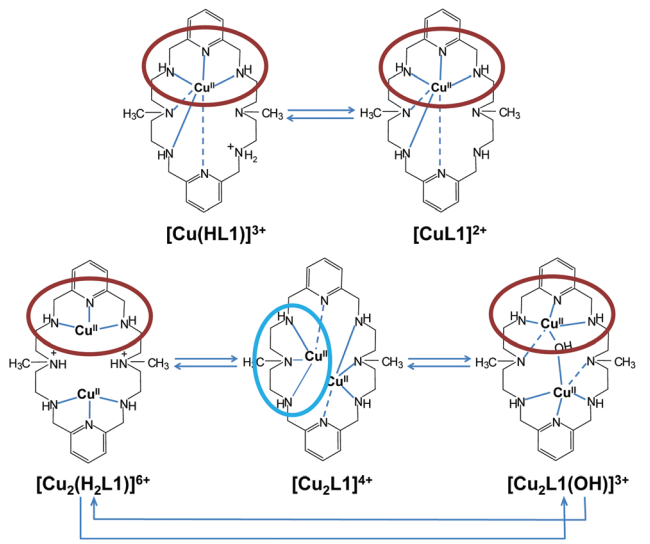

Fig. 10 Equilibrium model for the Cu^{2+}–**L1** system with the structure of the different species proposed on the basis of X-ray and kinetic data. Axial distances are represented with dotted lines.

An interesting situation arises for the interconversion between the $[Cu_2H_2(L1)]^{6+}$ and the $[Cu_2(L1)(OH)]^{3+}$ species, which should be fast if it occurs directly and slow if it goes through $[Cu_2(L1)]^{4+}$ as an intermediate. Experiments in which a solution containing one of these species is mixed with another solution buffered at the pH corresponding to maximum formation of the other species showed a shift of the absorption band within the stopped-flow mixing time. Although there were also slower spectral changes that probably correspond to the reaction with the buffer, these experiments suggest that the interconversion between $[Cu_2(H_2L1)]^{6+}$ and $[Cu_2(L1)(OH)]^{3+}$ does not necessarily go through the intermediate formation of $[Cu_2(L1)]^{4+}$.

The kinetics of the acid-promoted decomposition of Cu–L2 complexes

In the case of the **L2** complexes, the situation is more complicated. As pointed out above, the actual values of the equilibrium constants lead to complex mixtures of species at Cu : **L2** molar ratios of 1 : 1 and 2 : 1, so that it is not possible to select pH values in which one of the species exists with more than

90% abundance. In addition, no crystal structure could be obtained in this case, surely because the complex composition of the solutions also hinders adequate crystallization. To obtain some information on the individual species, solutions with both molar ratios were prepared and their electronic spectra recorded at selected pH values (see ESI†). The spectra of the different species were then calculated using the composition of the solutions obtained from the equilibrium data. In general all the mono and binuclear species show the maximum at wavelengths between 645 and 710 nm, the value increasing with the protonation state (see Table S5†). The wavelength range is similar for the mono and the binuclear complexes, although the intensity in the latter complexes is in general higher, which suggest that binuclear complexes contain both metal centers in coordination environments similar to those found in the mononuclear species. Moreover, the similarity of the spectra for the Cu^{2+} complexes with the **L1** and **L2** ligands indicates that the structures adopted by the different Cu–**L2** species are probably quite similar to those found for the **L1** complexes. Of special relevance is the fact that the $[Cu(H_3L2)]^{5+}$ species shows the absorption band at 700 nm. The analogous species with **L1** is not stable enough to be detected in the potentiometric studies but a protonated intermediate with a band at this wavelength is observed during the decomposition of the different Cu^{2+}–**L1** species, and the similarity of the spectra adds further support to the assumption that the intermediate is $[Cu(H_3L1)]^{5+}$.

The kinetics of decomposition of the **L2** complexes was studied using different starting conditions, and the results show that there are both similarities and differences with respect to the related **L1** complexes. The major similarity consists in the formation of an intermediate with a band at 700 nm within the stopped-flow mixing time. In the case of **L2**, formation of this intermediate was rapid under all the experimental conditions of the starting solution tried, so that it appears that for this ligand there is no species decomposing with a singular behavior as that observed for $[Cu_2(L1)]^{4+}$.[23] On the other hand, the major difference with respect to the **L1** complexes is the observation of a larger number of kinetic steps in the decomposition of the Cu–**L2** complexes, so that up to four kinetic steps can be resolved. Thus, in addition to the rapid step occurring within the stopped-flow mixing time, an adequate fit of the spectral changes using global analysis of the data required a model with three consecutive steps (for an example of experimental changes, calculated spectra and traces showing the quality of the fit, see the ESI†). Although decomposition of copper–polyamine complexes usually involves the breaking of several Cu–N bonds, to our knowledge there is no example in which the number of resolved kinetic steps is so large that it almost coincides with the number of Cu–N bonds to be broken. Moreover, as the starting solutions contain mixtures of species that decompose with polyphasic kinetics, in some cases there are difficulties in determining the pH dependence of the rate constants for the different steps.

This is especially evident for decomposition of solutions containing mixtures of binuclear species, for which no definitive

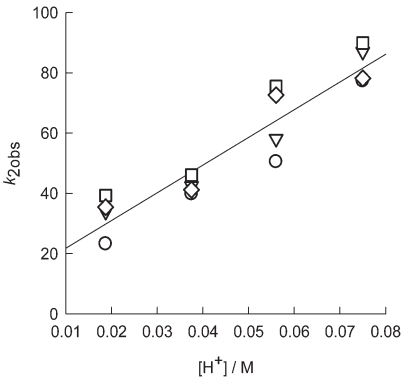

Fig. 11 Plot of the acid dependence for the observed rate constant corresponding to the second step in the acid-promoted decomposition of solutions containing mixtures of mononuclear Cu^{2+}–**L2** complexes. The starting solutions always contain Cu^{2+} and **L2** ions in a 1:1 molar ratio, the initial pH being adjusted to 3.36 (circles), 5.23 (triangles), 7.44 (squares), and 9.60 (diamonds).

conclusions could be obtained. Four steps could be always resolved in the kinetics of decomposition of the mononuclear species, the first one occurring within the stopped-flow mixing time and leading to the intermediate with a band at 698 nm and a molar absorptivity of *ca.* 145 M^{-1} cm^{-1}. The rate constants for the second step show a linear dependence with respect to the acid (see Fig. 11), the fit to eqn (2) leading to $a = 13 \pm 5$ s^{-1} and $b = (9.2 \pm 0.9) \times 10^2$ M^{-1} s^{-1}. The intermediate formed in this step shows a band at 712 nm with a molar absorptivity of *ca.* 105 M^{-1} cm^{-1}. The rate constant for the third resolved kinetic step is independent of the acid concentration ($k_{3obs} = 1.2 \pm 0.1$ s^{-1}) and leads to an intermediate with a band at *ca.* 725 nm and a molar absorptivity of *ca.* 60 M^{-1} cm^{-1}. The fourth step is also independent of the acid concentration, $k_{4obs} = (6.7 \pm 0.2) \times 10^{-2}$ s^{-1}, and leads to an intermediate with a band at 750 nm and a molar absorptivity of *ca.* 28 M^{-1} cm^{-1}.

One of the most striking observations when the kinetics of decomposition of the copper complexes with the **L1** and **L2** ligands is compared is the rapid formation of the intermediate with a band at 700 nm, which presumably corresponds to the $[Cu(H_3L)]^{5+}$ species.[24] With respect to the coordination environment of the metal centre in this intermediate, the comments above for the **L1** complexes suggest that Cu is coordinated to a damp subunit. However, the absorption band for the binuclear $[Cu_2([20]py_2N_4)(H_2O)_4]^{4+}$ complex, whose crystal structure shows two Cu–damp subunits,[25] appears at 630 nm, far from the 700 nm found for the $[Cu(H_3L)]^{5+}$ species. However, it has been shown for a series of related binuclear $[Cu_2([n]py_2N_4)]^{4+}$ complexes that the position of the band is strongly dependent on the size of the macrocycle, the maximum being observed at 665, 630, 635, 650 and 660 nm for $n = 18$, 20, 22, 24 and 26, respectively.[25] These data indicate that the position of the band can change significantly with minor changes in the structure of the macrocycle. Another significant difference between **L1** and **L2** is the different rate of

decomposition of the corresponding $[Cu(H_3L)]^{5+}$ intermediates, the process being about two orders of magnitude faster for **L2**. This increased lability of the Cu–N bonds is probably related to a more strained structure in the case of $[Cu(H_3L2)]^{5+}$, but the observation of polyphasic kinetics for decomposition of $[Cu(H_3L2)]^{5+}$ and not for the related **L1** species suggests that the subsequent intermediates with a higher protonated state are less strained in the case of **L2**.

Conclusions

The results of the present paper reveal interesting aspects of the chemistry of binucleating macrocyclic ligands from the thermodynamic, structural and kinetic points of view. Thus, the potentiometric data indicate that increasing methylation leads to a decrease in the stability of the mono and binuclear complexes that parallels the decrease in the overall basicity of the ligand. From the structural point of view, the Cu–**L1** system represents one of the best described systems because the crystal structures of up to three different species are available. Moreover, the structures reveal changes in the coordination mode of the ligand as a consequence of the changes in nuclearity and protonation degree. These changes are probably more favoured in the present case because the actual structure of the ligands makes interchangeable the donor subunits and the spacers. A correlation between the structure and the kinetics of decomposition of the Cu complexes has been observed, so that complex decomposition always starts with the breaking of the weakest Cu–N bonds. However, because of the different coordination modes of the ligand, different intermediates can be formed and this can result in significant changes in the kinetics of decomposition, so that kinetic changes can be used to detect changes in the coordination modes.

Experimental

Synthesis of compounds

L1·6HCl·5H$_2$O. The ligand **L1** was prepared using the literature procedure.[4] 2,6-Pyridine-dicarboxaldehyde (0.50 g, 3.70 mmol) dissolved in 100 mL of anhydrous ethanol was added to a solution of 2,2′-diamino-*N*-methyldiethylamine (0.43 g, 3.70 mmol) in anhydrous ethanol and was stirred for 2 h. $NaBH_4$ (1.39 g, 37 mmol) was then added portionwise. The mixture was stirred for 2 h at room temperature and the solvent was vacuum evaporated to dryness. The residue was treated with 50 mL of water and extracted with CH_2Cl_2 (3 × 40 mL). The organic phase was dried with anhydrous sodium sulfate and the solvent evaporated to dryness. The resulting oil was dissolved in anhydrous ethanol and **L1** was precipitated as its hexahydrochloride salt with hydrogen chloride solution (4.0 M in dioxane) (92% yield). Mp: 258–264 decomp. MS (*m*/*z*; ESI): 441.3, $[M + H]^+$. ^{1}H NMR (300 MHz, D_2O): δ (ppm), 7.91 (t, 2H, J = 7.85 Hz), 7.445 (d, 4H, J = 7.8 Hz), 4.53 (s, 8H), 3.70 (m, 16H), 2.91 (s, 6H). ^{13}C NMR (75 MHz, D_2O): δ (ppm), 150.55, 139.89, 123.35, 53.73, 51.33, 43.13, 40.06. Anal. Calcd for $C_{24}H_{40}N_8$·6HCl·5H_2O: C, 38.59; H, 7.56; N, 15.01. Found: C, 38.5; H, 7.2; N, 14.7.

Synthesis of L2·6HCl·3H$_2$O·EtOH. **L1** (2.0 g, 2.67 mmol) was dissolved in formic acid (3.25 mL, 74.7 mmol) in a 25 mL round flask. Formaldehyde 36% (2.70 mL, 32.02 mmol) and water (0.229 mL) were then added. The solution was refluxed for 72 hours. The flask was placed in an ice bath and a few drops of a concentrated NaOH solution were added until an oil appeared. The product was extracted with CH_2Cl_2 (3 × 20 mL). The organic phase was dried over $NaSO_4$. Then it was filtered and the solvent was removed under reduced pressure. A yellowish oil was obtained, which was purified by column chromatography over alumina (CH_2Cl_2–MeOH–isopropylamine, 80 : 12 : 8). 900 mg of **L2** (67% yield). MS (*m*/*z*): 497.30, $[M + H]^+$. ^{1}H NMR (300 MHz, $CDCl_3$): δ (ppm), 7.53 (t, J = 7.66 Hz, 2H), 7.23 (d, J = 7.67 Hz, 4H), 3.61 (s, 8H), 2.49 (m, 16H), 2.28–2.25 (m, 18H). ^{13}C NMR (75 MHz, $CDCl_3$): δ (ppm), 158.71, 136.78, 121.51, 64.22, 55.49, 54.75, 43.75, 43.64. Anal. Calcd For $C_{28}H_{48}N_8$·6HCl·3H_2O·CH_3CH_2OH: C, 44.18; H, 8.16; Cl, 26.08; N, 13.74; O, 7.84. Found: C, 44.0; H, 8.1; N, 13.7.

L1·6HCl·6H$_2$O (1). Crystals of **1** suitable for X-ray analysis were grown by slow evaporation of an acidic aqueous solution (pH = 2) containing **L1** in an open vessel. Anal. Calcd for: $C_{24}H_{58}Cl_6N_8O_6$: C, 37.68; H, 7.64; N, 14.65. Found: C, 37.7; H, 7.7; N, 15.0.

[Cu$_2$(L1)Cl$_2$](CF$_3$SO$_3$)$_2$ (2). Crystals of **2** were obtained by slow evaporation of an aqueous solution containing **L1** and $Cu(CF_3SO_3)_2$ at pH 8 with an excess of $Cu(CF_3SO_3)_2$. Anal Calcd for: $C_{26}H_{40}Cl_2Cu_2F_6N_8O_6S_2$: C, 33.33; H, 4.30; N, 11.96. S, 6.84. Found: C, 33.4; H, 5.0; N, 12.1; S, 6.9.

[Cu$_2$(L1)(OH)](ClO$_4$)$_3$·3H$_2$O (3). Crystals of **3** were grown by slow evaporation of aqueous solutions containing **L1** and $Cu(ClO_4)_2$·6H_2O in a 1 : 2 mole ratio at pH 9 in an open vessel. After several days, blue crystals of **3** suitable for X-ray diffraction were obtained. Anal. Calcd for $C_{24}H_{47}Cl_3Cu_2N_8O_{16}$: C, 30.83; H, 5.07; N, 11.99. Found: C, 30.9; H, 4.9; N, 12.0.

[Cu(L1)](ClO$_4$)$_2$ (4). Crystals of **4** were obtained following the same procedure as that for crystals **3**, but this time the **L1** : Cu mole ratio was adjusted to 1 : 1. Anal. Calcd for $C_{24}H_{40}Cl_2CuN_8O_8$: C, 41.07; H, 5.74; N, 15.97. Found: C, 41.3; H, 5.4; N, 16.1.

X-Ray crystallography

For the data collection of compounds **1** and **2**, an Oxford Xcalibur3 diffractometer with a CCD area detector was employed using MoKα radiation (λ = 0.71073 Å) at 120 K. The data collection was performed using CRYSALISPRO software.[26] For compounds **3** and **4**, an Enraf Nonius KappaCCD diffractometer with a CCD area detector was employed for data collection using MoKα radiation (λ = 0.71073 Å) at 293 K. The data collection was performed using Denzo software.[27] The structures were solved by direct methods using SIR92[28] and refined by full-matrix least squares on F^2 (SHELXL-97)[29] with Olex2.[30] All non-hydrogen atoms were refined anisotropically. The hydro-

gen atom positions were located in a difference Fourier map and then refined freely. MERCURY plots are shown with thermal ellipsoids at the 50% probability level. CIF files of **1–4** are deposited in CCDC with numbers 1009322–1009325.

Electromotive force measurements

The potentiometric titrations were carried out at 298.1 ± 0.1 K using NaCl 0.15 M as the supporting electrolyte. The experimental procedure (burette, potentiometer, cell, stirrer, microcomputer, *etc*.) has been fully described elsewhere.[31] The emf data were acquired with the computer program PASAT.[32] The reference electrode was an Ag/AgCl electrode in saturated KCl solution. The glass electrode was calibrated as a hydrogen-ion concentration probe by titration of previously standardized amounts of HCl with CO_2-free NaOH solutions and determining the equivalent point by Gran's method,[33] which gives the standard potential, $E^{\circ\prime}$, and the ionic product of water ($pK_w = 13.73(1)$).

The computer program HYPERQUAD[34] was used to fit the protonation and stability constants. Solutions containing the ligand salts with concentrations ranging from 1×10^{-3} to 5×10^{-3} M and with Cu^{2+} : L molar ratios varying from 2 : 1 to 1 : 2 were titrated with NaOH. The different titration curves for each ligand were treated as separated curves without significant variations in the values of the stability constants. Finally, the sets of data were merged together and treated simultaneously to give the final stability constants.

Kinetics

Kinetic studies of the acid-promoted complex decomposition were carried out at 298.1 ± 0.1 K with an Applied Photophysics SX17MV stopped-flow instrument provided with a PDA.1 diode array detector. The experiments were carried out under pseudo first order conditions of acid excess (0.02–0.10 M HCl, complex concentration *ca.* 2×10^{-4} M). The ionic strength was maintained using 0.15 M NaCl. The spectral changes with time were recorded using the standard software of the instrument and analyzed using the Specfit program.[35]

Acknowledgements

Financial support by the Spanish Ministerio de Economía y Competitividad and the FEDER programme of the E.U. (grants CTQ2012-37821-C02-02 and CTQ2013-48917-C3-1-P), Consolider-Ingenio 2010 Program (grant CSD2010-00065) and Generalitat Valenciana PROMETEO GVA 2011-008 is gratefully acknowledged.

Notes and references

1 (*a*) V. L. Goedken and D. H. Busch, *J. Am. Chem. Soc.*, 1972, **94**, 7355; (*b*) F. R. Keene, *Coord. Chem. Rev.*, 1999, **187**, 121.
2 A. Casitas and X. Ribas, *Chem. Sci.*, 2013, **4**, 2301.
3 H. Fenniri, C. Dallaire, D. P. Funeriu and J. M. Lehn, *J. Chem. Soc., Perkin Trans. 2*, 1997, 2073.
4 (*a*) R. J. Motekaitis, A. E. Martell, J. P. Lecomte and J. M. Lehn, *Inorg. Chem.*, 1983, **22**, 609; (*b*) M. G. B. Drew, B. P. Murphy, J. Nelson and S. M. Nelson, *J. Chem. Soc., Dalton Trans.*, 1987, 873; (*c*) C. Anda, A. Llobet, A. E. Martell, J. Reibenspies, E. Berni and X. Solans, *Inorg. Chem.*, 2004, **43**, 2793; (*d*) R. Menif, A. E. Martell, P. J. Squattrito and A. Clearfield, *Inorg. Chem.*, 1990, **29**, 4723.
5 (*a*) J. R. J. Sorenson and W. Hangarter, *Inflammation*, 1977, **2**, 217; (*b*) B. Sarkar, *Chem. Rev.*, 1999, **99**, 2535; (*c*) K. G. Daniel, P. Gupta, R. H. Harbach, W. C. Guida and Q. P. Dou, *Biochem. Pharmacol.*, 2004, **67**, 1139; (*d*) T. Wang and Z. Guo, *Curr. Med. Chem.*, 2006, **13**, 525.
6 (*a*) M. Shokeen and C. J. Anderson, *Acc. Chem. Res.*, 2009, **42**, 832; (*b*) D. J. Stigers, R. Ferdani, G. R. Weisman, E. H. Wong, C. J. Anderson, J. A. Golen, C. Moore and A. L. Rheingold, *Dalton Trans.*, 2010, **39**, 1699; (*c*) M. G. Basallote, C. E. Castillo, M. A. Máñez, P. Lubal, M. Martínez, C. Rodríguez and J. Vaněk, *Inorg. Chem. Commun.*, 2010, **13**, 1272; (*d*) T. J. Wadas, E. H. Wong, G. R. Weismann and C. J. Anderson, *Chem. Rev.*, 2010, **110**, 2858.
7 (*a*) B. F. Liang and C. S. Chung, *Inorg. Chem.*, 1981, **20**, 2152; (*b*) J. W. Chen, D. S. Wu and C. S. Chung, *Inorg. Chem.*, 1986, **25**, 1940; (*c*) H. Sun, H. Lin, S. Zhu, G. Zhao, X. Su and Y. Chen, *Polyhedron*, 1999, **18**, 1045.
8 L. H. Chen and C. S. Chung, *Inorg. Chem.*, 1988, **27**, 1880.
9 (*a*) M. S. Chao and C. S. Chung, *Inorg. Chem.*, 1989, **28**, 686; (*b*) L. H. Chen and C. S. Chung, *Inorg. Chem.*, 1989, **28**, 1402.
10 (*a*) P. Díaz, M. G. Basallote, M. A. Máñez, E. García-España, L. Gil, J. Latorre, C. Soriano, B. Verdejo and S. V. Luis, *Dalton Trans.*, 2003, 1186; (*b*) J. Aguilar, M. G. Basallote, L. Gil, J. C. Hernandez, M. A. Máñez, E. García-España, C. Soriano and B. Verdejo, *Dalton Trans.*, 2004, 94; (*c*) B. Verdejo, A. Ferrer, S. Blasco, C. E. Castillo, J. González, J. Latorre, M. A. Máñez, M. G. Basallote, C. Soriano and E. García-España, *Inorg. Chem.*, 2007, **46**, 5707; (*d*) B. Verdejo, M. G. Basallote, A. Ferrer, M. A. Mañez, J. C. Hernández, M. Chadim, J. Hodacová, J. M. Llinares, C. Soriano and E. García-España, *Eur. J. Inorg. Chem.*, 2008, 1497; (*e*) A. G. Algarra, M. G. Basallote, C. E. Castillo, M. P. Clares, A. Ferrer, E. García-España, J. M. Llinares, M. A. Máñez and C. Soriano, *Inorg. Chem.*, 2009, **48**, 902; (*f*) A. Mendoza, J. Aguilar, M. G. Basallote, L. Gil, J. C. Hernández, M. A. Máñez, E. García-España, L. Ruiz-Ramírez, C. Soriano and B. Verdejo, *Chem. Commun.*, 2003, 3032.
11 (*a*) A. Bencini, A. Bianchi, E. García-España, M. Micheloni and J. A. Ramirez, *Coord. Chem. Rev.*, 1999, **188**, 97; (*b*) J. E. Sarneski, H. L. Surprenant, F. K. Molen and C. N. Reilley, *Anal. Chem.*, 1975, **47**, 2116; (*c*) C. Frassineti, L. Alderighi, P. Gans, A. Sabatini, A. Vacca and S. Ghelli, *Anal. Bioanal. Chem.*, 2003, **376**, 1041; (*d*) C. Frassineti, S. Ghelli, P. Gans, A. Sabatini, M. S. Moruzzi and A. Vacca, *Anal. Biochem.*, 1995, **231**, 374.

12 (*a*) J. Aragó, A. Bencini, A. Bianchi, E. García-España, M. Micheloni, P. Paoletti, J. A. Ramírez and A. Rodríguez, *J. Chem. Soc., Dalton Trans.*, 1991, 3077; (*b*) R. Belda, S. Blasco, B. Verdejo, H. R. Jiménez, A. Doménech-Carbó, C. Soriano, J. Latorre, C. Terencio and E. García-España, *Dalton Trans.*, 2013, **42**, 1194; (*c*) A. Bencini, A. Bianchi, P. Paoletti and P. Paoli, *Coord. Chem. Rev.*, 1992, **120**, 51; (*d*) G. Ambrosi, M. Formica, V. Fusi, L. Giorgi, E. Macedi, M. Micheloni, P. Paoli and P. Rossi, *Inorg. Chem.*, 2009, **48**, 10424; (*e*) C. Bazzicalupi, A. Bencini, A. Bianchi, L. Borsari, A. Danesi, C. Giorgi, C. Lodeiro, P. Mariani, F. Pina, S. Santarelli, A. Tamayo and B. Valtancoli, *Dalton Trans.*, 2006, 4000.

13 (*a*) E. K. Barefield, G. M. Freeman and D. G. Van Derveer, *Inorg. Chem.*, 1986, **25**, 552; (*b*) R. D. Hancock and A. E. Martell, *Chem. Rev.*, 1989, **89**, 1875; (*c*) G. Golub, H. Cohen and D. Mayerstein, *J. Chem. Soc., Chem. Commun.*, 1992, 397.

14 (*a*) S. J. Archibald, *Annu. Rep. Prog. Chem., Sect. A*, 2010, **106**, 295; (*b*) S. P. de Visser, J.-U. Rohdeb, Y.-M. Leec, J. Choc and W. Nam, *Coord. Chem. Rev.*, 2013, **257**, 381; (*c*) M. Costas, M. P. Mehn, M. P. Jensen and L. Que Jr., *Chem. Rev.*, 2004, **104**, 939.

15 (*a*) L. Branco, J. Costa, R. Delgado, M. G. B. Drew, V. Félix and B. J. Goodfellow, *J. Chem. Soc., Dalt. Trans.*, 2002, 3539; (*b*) G. R. Newkome, V. K. Majestic and F. R. Fronczek, *Inorg. Chim. Acta*, 1983, **77**, L47; (*c*) L. H. Bryant, A. Lachgar, K. S. Coates and S. C. Jackels, *Inorg. Chem.*, 1994, **33**, 2219; (*d*) J. M. Martínez-Sánchez, R. Bastida de la Calle, A. Macías, P. Pérez-Lourido and L. Valencia Matarranz, *Polyhedron*, 2006, **25**, 3495.

16 Q. Lu, R. I. Carroll, J. H. Reibenspies, A. E. Martell and A. Clearfield, *J. Mol. Struct.*, 1998, **470**, 121.

17 A. W. Addison, T. N. Rao, J. Reedijk, J. van Rijn and G. C. Verschoor, *J. Chem. Soc., Dalton Trans.*, 1984, 1349.

18 (*a*) C. Núñez, R. Bastida, L. Lezama, A. Macías, P. Lérez-Lourido and L. Valencia, *Inorg. Chem.*, 2011, **50**, 5596; (*b*) C. Núñez, R. Bastida, A. Macías, L. Valencia, N. I. Neuman, A. C. Rizzi, C. D. Brondino, P. J. González, J. L. Capelo and C. Lodeiro, *Dalton Trans.*, 2010, **39**, 11654.

19 M. J. Fernández-Trujillo, B. Szpoganicz, M. A. Máñez, L. T. Kist and M. G. Basallote, *Polyhedron*, 1996, **15**, 3511.

20 (*a*) D. K. Cabbiness and D. W. Margerum, *J. Am. Chem. Soc.*, 1969, **91**, 6540; (*b*) A. Read and D. W. Margerum, *Inorg. Chem.*, 1981, **20**, 3143.

21 S. Siddiqui and R. E. Shepherd, *Inorg. Chem.*, 1983, **22**, 3726.

22 (*a*) M. G. Basallote, J. Durán, M. J. Fernández-Trujillo and M. A. Máñez, *Polyhedron*, 2001, **20**, 75; (*b*) M. G. Basallote, J. Durán, M. J. Fernández-Trujillo, M. A. Máñez, M. Quirós and J. M. Salas, *Polyhedron*, 2001, **20**, 297.

23 The only cases in which there is no rapid shift of the absorption band within the mixing time are those in which the band already appears at *ca.* 700 nm, *i.e.* the binuclear $[Cu_2(H_2L2)]^{6+}$ and the mononuclear $[Cu(H_3L2)]^{5+}$ species.

24 Although the molar absorptivities found for the **L1** and **L2** intermediates are significantly different, the differences can be understood on the basis of the different nature of the compounds, the complex mixtures of species formed, and the accumulation of experimental and fitting errors.

25 F. Li, R. Delgado, J. Costa, M. G. B. Drew and V. Felix, *Dalton Trans.*, 2005, 82.

26 *Agilent, CrysAlis PRO*, Agilent Technologies UK Ltd, Yarnton, England, 2011.

27 Z. Otwinowski and W. Minor, "Processing of X-ray Diffraction Data Collected in Oscillation Mode", in Methods in Enzymology, *Volume 276: Macromolecular Crystallography*, ed. C. W. Carter Jr. and R. M. Sweet, Academic Press, New York, 1997, part A, pp. 307–326.

28 A. Altomare, M. C. Burla, M. Cavalli, G. Cascarano, C. Giacovazzo, A. Gagliardi, A. G. Moliterni, G. Polidori and R. Spagna, *Sir97: "A New Program for Solving and Refining Crystal Structures"*, Istituto di Ricerca per lo Sviluppo di Metodologie Cristallografiche CNR, Bari, 1997.

29 G. M. Sheldrick, *Acta Crystallogr., Sect. A: Fundam. Crystallogr.*, 2008, **64**, 112.

30 O. V. Dolomanov, L. J. Bourhis, R. J. Gildea, J. A. K. Howar and H. Puschmann, *J. Appl. Crystallogr.*, 2009, **42**, 339.

31 E. García-España, M. J. Ballester, F. Lloret, J. M. Moratal, J. Faus and A. Bianchi, *J. Chem. Soc., Dalton Trans.*, 1988, 101.

32 M. Fontanelli and M. Micheloni, Proceedings of the I Spanish-Italian Congress on Thermodynamics of Metal Complexes, Diputación de Castellón, Spain, 1990.

33 (*a*) G. Gran, *Analyst*, 1952, **77**, 661; (*b*) F. J. C. Rossotti and H. Rossotti, *J. Chem. Educ.*, 1965, **42**, 375.

34 P. Gans, A. Sabatini and A. Vacca, *Talanta*, 1996, **43**, 1739.

35 R. A. Binstead, B. Jung and A. D. Zuberbühler, *SPECFIT-32, Spectrum Software Associates*, Chapel Hill, 2000.

